J|A|C|S
ARTICLES
Published on Web 02/19/2004

Peroxovanadate Imidazole Complexes as Catalysts for Olefin Epoxidation: Density Functional Study of Dynamics, ^{51}V NMR Chemical Shifts, and Mechanism

Michael Bühl,* Rachel Schurhammer,† and Petra Imhof‡

Contribution from the Max-Planck-Institut für Kohlenforschung, Kaiser-Wilhelm-Platz 1, D-45470 Mülheim an der Ruhr, Germany

Received November 5, 2003; E-mail: buehl@mpi-muelheim.mpg.de

Abstract: A density functional study of $[VO(O_2)_2(Im)]^-$ (**1**, Im = imidazole) is presented, calling special attention to effects of dynamics and solvation on the ^{51}V chemical shift. According to Car−Parrinello molecular dynamics simulations, rotation of the Im ligand can be fast in the gas phase, but is more hindered in aqueous solution. In the latter, bonding between Im and V is reinforced, and dynamic averaging of GIAO-B3LYP magnetic shieldings affords a gas-to-liquid shift of ca. −100 ppm for $\delta(^{51}V)$. A complete catalytic cycle has been characterized for olefin epoxidation mediated by **1**, using H_2O_2 as oxidant. The rate-determining step is indicated to be initial oxygen atom transfer from **1** to the substrate via a spiro-like transition state. Substituent effects on this barrier are examined, and a significant decrease (by 2−6 kcal/mol) is revealed upon removal of the Im proton or upon complexation with a H-bond acceptor. Implications for the mechanism of the oxidative chemistry of vanadium-dependent haloperoxidases and requirements for prospective biomimetic analogues are discussed.

Introduction

Oxidation of organic substrates is potentially very useful, but is usually difficult to control. Significant research efforts have been and are being made to widen the applicability of oxidation reactions by increasing their selectivity.[1] Despite impressive progress in the level of understanding of such reactions, which has led to some industrial applications,[2] their practical use is often still quite limited. In attempts to borrow know-how from nature, the study of so-called biomimetic or bioinspired reagents is enjoying increasing popularity.[3,4] The goal is to mimic the high activity and selectivity of enzymes by designing simpler models of their active sites. Many natural oxidases contain one or more transition metals in the active center, prominent examples being the cytochrome P450 family,[5] copper-based metalloproteins,[6] or vanadium-dependent haloperoxidases.[7] The latter define one of the principal areas of the bioinorganic chemistry of vanadium.[8,9] The discovery that certain model compounds for these haloperoxidases show physiological activity as insulin mimetics[10] has stimulated numerous studies to elucidate the details of the underlying biological functions. The haloperoxides themselves catalyze a variety of oxidation reactions, for instance, the oxidation of bromide to hypobromite (from which the name of the enzymes was coined), the transformation of organic sulfides to sulfoxides, or the epoxidation of olefins, using different oxygen sources, such as air or hydrogen peroxide.[11] These transformations are particularly attractive from a synthetic point of view if the stereocontrol typical for enzymatic reactions can be fully exploited.

For a rational design of biomimetic analogues, detailed knowledge of the elementary steps involved is desirable. Even though the solid-state structure of a vanadium-containing haloperoxidase is known both in the native and in the peroxo form (Scheme 1),[12] the mechanistic details of the oxidation process are not established. The current view is that the peroxo form, presumably activated by a hydrogen bond from a neighboring lysine residue, is the active oxidant. Numerous

† Present address: Université Louis Pasteur, Laboratoire MSM − UMR 7551, 4 rue Blaise Pascal, F-67070 Strasbourg Cedex, France.

‡ Present address: Interdisziplinäres Zentrum für Wissenschaftliches Rechnen, Universität Heidelberg, Im Neuenheimer Feld 368, D-69120 Heidelberg, Germany.

(1) For example: (a) Barton, D., Martell, A. E., Sawyer, D. T., Eds. *The Activation of Dioxygen and Homogeneous Catalytic Oxidation*; Plenum Press: New York, 1993. (b) Shilov, A. E.; Shul'pin, G. B. *Chem. Rev.* **1997**, *97*, 2879−2932.
(2) Brégeault, J.-M. *Dalton Trans*. **2003**, 3289−3302.
(3) For example: (a) Meunier, B., Ed. *Biomimetic Oxidations Catalyzed by Transition Metal Complexes*; Imperial College Press: London, 2000. (b) Gamez, P.; Aubel, P. G.; Driessen, W. L.; Reedijk, J. *Chem. Soc. Rev.* **2001**, *30*, 376−385.
(4) Oxidations with vanadium complexes: Ligtenbarg, A. G. J.; Hage, R.; Feringa, B. L. *Coord. Chem. Rev*. **2003**, *237*, 89−101.
(5) Ortiz de Montellano, P. R., Ed. *Cyctochrome P450: Structure, Mechanisms, and Biochemistry*, 2nd ed.; Plenum Press: New York, 1995.
(6) (a) Karlin, K. D., Tyeklár, Z., Eds. *Bioinorganic Chemistry of Copper*; Chapman & Hall: New York, 1993. (b) Klinmann, J. P. *Chem. Rev*. **1996**, *96*, 2541−2561. (c) Solomon, E. I.; Sundaram, U. M.; Machonkin, T. E. *Chem. Rev*. **1996**, *96*, 2563−2606.
(7) Butler, A.; Baldwin, A. H. *Struct. Bonding* **1997**, *89*, 109.
(8) (a) Crans, D. C. In *Metal Ions in Biological Systems*; Sigel, H., Sigel, A., Eds.; Marcel Dekker: New York, 1995; Vol. 31, pp 147−210. (b) Tracey, A. S., Crans, D. C., Eds. *Vanadium Compounds − Chemistry, Biochemistry, and Therapeutic Applications*; ACS Symposium Series, Vol. 711; American Chemical Society: Washington, DC, 1998.
(9) Review: Rehder, D. *Inorg. Chem. Commun*. **2003**, *6*, 604−617.
(10) Thompson, K. H.; McNeill, J. H.; Orvig, C. *Chem. Rev*. **1999**, *99*, 2561−2571.
(11) Review: Dembitsky, V. M. *Tetrahedron* **2003**, *59*, 4701−4720.
(12) (a) Messerschmidt, A.; Wever, R. *Proc. Natl. Acad. Sci. U.S.A.* **1996**, *93*, 392−396. (b) Messerschmidt, A.; Prade, L.; Wever, R. *Biol. Chem*. **1997**, *378*, 309−315.

10.1021/ja039436f CCC: $27.50

Scheme 1. Coordination about Vanadium in the Native (Top Left) and Peroxo Forms (Top Right) of the Fungal Peroxidase from *C. inaequaliz* (His = Histidine, H-Bond Pattern Not Shown); Bottom: Structural Model for the Peroxo Form

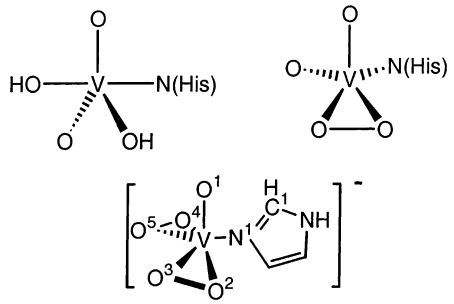

model compounds have been synthesized that preserve the coordination sphere of the metal in the enzyme as closely as possible.[13] The simplest analogue containing only oxo, peroxo, and aromatic N-donor ligands is probably $[VO(O_2)_2(Im)]^-$ (**1**, Im = imidazole), which has been characterized by X-ray crystallography,[14] and which is the predominant species of the vanadate/H_2O_2/Im system at low concentration and pH 7.[15]

Interest in **1** has concentrated mainly on its insulin-mimetic properties rather than peroxidase-like reactivity. Closely related compounds, however, have been shown to be active in olefin epoxidation.[16,17] We now report a computational study of this reaction using **1** as a model catalyst, calling special attention to the identification of the rate-determining step and to substituent effects on the corresponding activation barrier. From the intrinsic reactivity of this model system, important implications are to be expected for the key steps in the catalytic cycle of vanadium-containing peroxidases, and for ligand tuning in biomimetic complexes thereof.

Because ^{51}V NMR spectroscopy is an important analytical tool for diamagnetic vanadium complexes in general,[18] and for the abovementioned peroxovanadium(V) species in particular, we also report computed ^{51}V chemical shifts of **1** and its derivatives. Thermal and solvent effects on this property (experiments are usually conducted in water) are assessed using a molecular dynamics (MD)-based methodology, which we have introduced recently to model transition-metal chemical shifts in aqueous solution.[19] In this approach, MD simulations are performed for the substrate embedded in an array of discrete solvent molecules, and computed magnetic shieldings are averaged along the trajectory. Preliminary results for **1** have been communicated in a conference proceedings book[20] and are now fully documented here.

Computational Details

Stationary points were optimized with the Gaussian 98 program[21] at the BP86/AE1 level, that is, employing the exchange and correlation functionals of Becke[22] and Perdew,[23] respectively, together with a fine integration grid (75 radial shells with 302 angular points per shell), the augmented Wachters' basis[24] on V (8s7p4d, full contraction scheme 62111111/3311111/3111), and the 6-31G* basis[25] on all other elements. This and comparable DFT levels have proven quite successful for transition-metal compounds and are well suited for the description of structures, energies, barriers, etc.[26] The nature of the stationary points was verified by computations of the harmonic frequencies at that level. Transition states were characterized by a single imaginary frequency, and visual inspection of the corresponding vibrational modes ensured that the desired minima are connected. In cases of doubt, the key parts of the intrinsic reaction coordinate were followed. The computed harmonic frequencies were used to evaluate zero-point energies (ZPEs) and enthalpic and entropic corrections at 300 K. Single-point energy calculations were performed for the BP86/AE1 geometries at the BP86/AE1+ level, that is, with a basis augmented with diffuse functions on C, N, and O.[27] Energies are reported at the BP86/AE1+ level including BP86/AE1 ZPEs (denoted ΔE + ZPE; for selected ion−dipole complexes these include also a correction for basis-set superposition error with the counterpoise method[28] as implemented in Gaussian 03[29]); in addition, the estimated ΔG values are given as well. The basis sets are the same as those used in ref 19a.

Geometries of both rotamers of **1** were reoptimized using the density-functional based Car−Parrinello scheme[30] as implemented in the CPMD program,[31] until the maximum gradient was less than 5×10^{-4} au

(13) (a) Rehder, D. *Coord. Chem. Rev.* **1999**, *182*, 297−322. (b) Rehder, D.; Santoni, G.; Licini, G. M.; Schulzke, C.; Meier, B. *Coord. Chem. Rev.* **2003**, *237*, 53−63.
(14) Crans, D. C.; Keramidas, A. D.; Hoover-Litty, H.; Anderson, O. P.; Miller, M. M.; Lemoine, L. M.; Pleasic-Williams, S.; Vandenberg, M.; Rossomando, A. J.; Sweet, L. J. *J. Am. Chem. Soc.* **1997**, *119*, 5447−5448.
(15) (a) Andersson, I.; Angus-Dunne, S.; Howart, O.; Pettersson, L. *J. Inorg. Biochem.* **2000**, *80*, 51−58. (b) Review: Pettersson, L.; Andersson, I.; Gorzsás, A. *Coord. Chem. Rev.* **2003**, *237*, 77−87.
(16) With His or 3,5-dimethylpyrazole as coligands: Mukherjee, J.; Ganguly, S.; Bhattacharjee, M. *Indian J. Chem., Sect. A* **1996**, *35*, 471.
(17) Glas, H.; Herdtweck, E.; Artus, G. R. J.; Thiel, W. R. *Inorg. Chem.* **1998**, *37*, 3644.
(18) See, for instance: Rehder, D. In *Transition Metal Nuclear Magnetic Resonance*; Pregosin, P. S., Ed.; Elsevier: Amsterdam, 1991; pp 1−58.
(19) (a) Bühl, M.; Parrinello, M. *Chem.-Eur. J.* **2001**, *7*, 4487−4494. (b) Bühl, M.; Mauschick, F. T.; Terstegen, F.; Wrackmeyer, B. *Angew. Chem., Int. Ed.* **2002**, *41*, 2312−2315. (c) Bühl, M.; Mauschick, F. *Phys. Chem. Chem. Phys.* **2002**, *4*, 5508−5514. (d) Bühl, M. *J. Phys. Chem. A* **2002**, *106*, 10505−10509.
(20) Bühl, M.; Mauschick, F. T.; Schurhammer, R. In *High Performance Computing in Science and Engineering, Munich 2002*; Wagner, S., Hanke, W., Bode, A., Durst, F., Eds.; Springer: Berlin, 2003; pp 189−199.
(21) Frisch, M. J.; Trucks, G. W.; Schlegel, H. B.; Scuseria, G. E.; Robb, M. A.; Cheeseman, J. R.; Zakrzewski, V. G.; Montgomery, J. A.; Stratman, R. E.; Burant, J. C.; Dapprich, S.; Millam, J. M.; Daniels, A. D.; Kudin, K. N.; Strain, M. C.; Farkas, O.; Tomasi, J.; Barone, V.; Cossi, M.; Cammi, R.; Mennucci, B.; Pomelli, C.; Adamo, C.; Clifford, S.; Ochterski, J.; Petersson, G. A.; Ayala, P. Y.; Cui, Q.; Morokuma, K.; Malick, D. K.; Rabuck, A. D.; Raghavachari, K.; Foresman, J. B.; Cioslowski, J.; Ortiz, J. V.; Baboul, A. G.; Stefanov, B. B.; Liu, C.; Liashenko, A.; Piskorz, P.; Komaromi, I.; Gomperts, R.; Martin, R. L.; Fox, D. J.; Keith, T.; Al-Laham, M. A.; Peng, C. Y.; Nanayakkara, A.; Gonzalez, C.; Challacombe, M.; Gill, P. M. W.; Johnson, B. G.; Chen, W.; Wong, M. W.; Andres, J. L.; Gonzales, C.; Head-Gordon, M.; Replogle, E. S.; Pople, J. A. *Gaussian 98*; Gaussian, Inc.: Pittsburgh, PA, 1998.
(22) Becke, A. D. *Phys. Rev. A* **1988**, *38*, 3098−3100.
(23) Perdew, J. P. *Phys. Rev. B* **1986**, *33*, 8822−8824. Perdew, J. P. *Phys. Rev. B* **1986**, *34*, 7406.
(24) (a) Wachters, A. J. H. *J. Chem. Phys.* **1970**, *52*, 1033−1036. (b) Hay, P. J. *J. Chem. Phys.* **1977**, *66*, 4377−4384
(25) (a) Hehre, W. J.; Ditchfield, R.; Pople, J. A. *J. Chem. Phys.* **1972**, *56*, 2257−2261. (b) Hariharan, P. C.; Pople, J. A. *Theor. Chim. Acta* **1973**, *28*, 213−222.
(26) See, for instance: Koch, W.; Holthausen, M. C. *A Chemist's Guide to Density Functional Theory*; Wiley-VCH: Weinheim, 2000, and the extensive bibliography therein.
(27) Clark, T.; Chandrasekhar, J.; Spitznagel, G. W.; Schleyer, P. v. R. *J. Comput. Chem.* **1983**, *4*, 294.
(28) Boys, S. F.; Bernardi, F. *Mol. Phys.* **1970**, *19*, 553−566.
(29) Frisch, M. J.; Trucks, G. W.; Schlegel, H. B.; Scuseria, G. E.; Robb, M. A.; Cheeseman, J. R.; Montgomery, J. A., Jr.; Vreven, T.; Kudin, K. N.; Burant, J. C.; Millam, J. M.; Iyengar, S. S.; Tomasi, J.; Barone, V.; Mennucci, B.; Cossi, M.; Scalmani, G.; Rega, N.; Petersson, G. A.; Nakatsuji, H.; Hada, M.; Ehara, M.; Toyota, K.; Fukuda, R.; Hasegawa, J.; Ishida, M.; Nakajima, T.; Honda, Y.; Kitao, O.; Nakai, H.; Klene, M.; Li, X.; Knox, J. E.; Hratchian, H. P.; Cross, J. B.; Adamo, C.; Jaramillo, J.; Gomperts, R.; Stratmann, R. E.; Yazyev, O.; Austin, A. J.; Cammi, R.; Pomelli, C.; Ochterski, J. W.; Ayala, P. Y.; Morokuma, K.; Voth, G. A.; Salvador, P.; Dannenberg, J. J.; Zakrzewski, V. G.; Dapprich, S.; Daniels, A. D.; Strain, M. C.; Farkas, O.; Malick, D. K.; Rabuck, A. D.; Raghavachari, K.; Foresman, J. B.; Ortiz, J. V.; Cui, Q.; Baboul, A. G.; Clifford, S.; Cioslowski, J.; Stefanov, B. B.; Liu, G.; Liashenko, A.; Piskorz, P.; Komaromi, I.; Martin, R. L.; Fox, D. J.; Keith, T.; Al-Laham, M. A.; Peng, C. Y.; Nanayakkara, A.; Challacombe, M.; Gill, P. M. W.; Johnson, B.; Chen, W.; Wong, M. W.; Gonzalez, C.; Pople, J. A. *Gaussian 03*; Gaussian, Inc.: Pittsburgh, PA, 2003.
(30) Car, R.; Parrinello, M. *Phys. Rev. Lett.* **1985**, *55*, 2471−2474.
(31) Hutter, J.; Alavi, A.; Deutsch, T.; Bernasconi, M.; Goedecker, S.; Marx, D.; Tuckerman, M.; Parrinello, M. *CPMD Version 3.3a*; Max-Planck-Institut für Festkörperforschung and IBM Research Laboratory (1995−1999).

(denoted CP-opt). The BP86 functional was employed, together with norm-conserving pseudopotentials generated according to the Troullier and Martins procedure[32] and transformed into the Kleinman−Bylander form.[33] For vanadium, a semicore (or small-core) pseudopotential was generated corresponding to that used previously in conjunction with the BLYP functional. Test calculations ensured that very similar results (in terms of both geometrical parameters and chemical shifts) are obtained with both functionals.[20] Periodic boundary conditions were imposed using a cubic supercell with a box size of 11.5 Å. Kohn−Sham orbitals were expanded in plane waves up to a kinetic energy cutoff of 80 Ry. For the complexes in vacuo, Car−Parrinello molecular dynamics simulations were performed starting from the equilibrium structure, using a fictitious electronic mass of 600 au and a time step of 0.121 fs. Unconstrained simulations (NVE ensemble) were performed over 1.5 ps at ca. 300 K, the first 0.5 ps of which were taken for equilibration. For the aqueous solution, the box was filled with 48 water molecules. To increase the time step, hydrogen was substituted with deuterium. The system was equilibrated for 0.5 ps, maintaing a temperature of 300(±50) K, and was then propagated without constraints for 4 ps.

Magnetic shieldings were computed for equilibrium structures and for snapshots along the trajectories employing the B3LYP[34] hybrid functional, together with basis AE1+. Snapshots were taken every 20 fs over the last 1 ps. No periodic boundary conditions were employed, and solvent water molecules were not included specifically, but in the form of point charges employing values of −0.9313 and +0.4656 for O and H atoms, respectively, as obtained for a single water molecule from natural population analysis[35] at the B3LYP/6-31G* level (water molecules from the six adjacent boxes were also included as point charges; cf., the procedure in ref 19a). These computations were carried out with the Gaussian 98 program package.[21] Chemical shifts are reported relative to $VOCl_3$, optimized or simulated at the same respective level (σ values of −2319 and −2264 ppm employing BP86/AE1 and CP-opt geometries, respectively, and −2292 ppm for a CPMD simulation averaged over 1 ps).

Results and Discussion

This section is organized as follows: First, we present a computational characterization of the catalyst complex **1**, calling special attention to the structure and $\delta(^{51}V)$ value in aqueous solution. In the second part, we investigate possible mechanisms for olefin epoxidation mediated by **1** to identify the rate-determining step of this process. Finally, substituent effects and their implications for the reactivity of vanadium-dependent haloperoxidases are discussed.

(1) Structure, Dynamics, and ^{51}V Chemical Shift of 1. Geometrical parameters for **1** are summarized in Table 1 (see Scheme 1 for numbering scheme). The computed equilibrium geometries (BP86/AE1 and CP-opt entries) are in good mutual accord, despite the different computational setup (all-electron vs pseudopotential calculations, isolated molecule vs periodic boundary conditions, etc.). On going from the static to the dynamically averaged values in the gas phase, most bond lengths are somewhat elongated (compare CP-opt and CPMD entries). This elongation is less pronounced for the VO bonds (typically below 0.01 Å), but is more prominent for the V−N distance (0.02 Å). The most notable change is found for the orientation of the Im group, as assessed by the OVNC dihedral angle θ. Large fluctuations are found at 300 K, and the average value increases from ca. 90° to 110°.

Table 1. Selected Geometrical Parameters (Distances in Å, Bond and Dihedral Angles in deg) of **1** (See Scheme 1 for Numbering)

parameter	BP86/AE1	CP-opt[a]	CPMD[a,b]	CPMD/D_2O[b,c]	expt.[d]
$r(V-N^1)$	2.189	2.166	2.186(47)	2.091(60)	2.092(2)
$r(V-O^1)$	1.634	1.616	1.621(23)	1.621(28)	1.603(2)
$r(V-O^2)$	1.872	1.885	1.887(54)	1.886(47)	1.866(2)
$r(V-O^3)$	1.896	1.902	1.904(39)	1.914(53)	1.884(2)
$r(V-O^4)$	1.878	1.890	1.896(53)	1.889(44)	1.865(2)
$r(V-O^5)$	1.901	1.904	1.901(37)	1.915(48)	1.922(2)
$r(O^2-O^3)$	1.467	1.487	1.488(17)	1.490(52)	1.467(3)
$r(O^4-O^5)$	1.468	1.487	1.487(20)	1.493(33)	1.475(2)
$a(O^1-V-N^1)$	93.0	93.6	94.3(38)	96.5(50)	95.5
$\theta(O^1-V-N^1-C^1)$	89.3	89.5	110(7)	90(23)	28.3

[a] In vacuo. [b] In parentheses: standard deviation along the trajectory. [c] In water. [d] X-ray with ImH^+ counterion and one crystal water per unit cell, from ref 14 (in parentheses: experimental uncertainties).

Upon immersion of **1** in water, only small further changes occur for most averaged parameters, except for θ, which shows even larger fluctuations, and the VN bond length, which is significantly decreased (by 0.1 Å, Table 1). A similar reinforcement of the bonding upon solvation has been noted between the metal and the water ligand in the closely related $[VO(O_2)_2(OH_2)]^-$ (**2**).[19a] The VN bond distance simulated for aqueous **1** is in good accord with the value observed for this ion in the solid state (Table 1, compare CPMD/D_2O and expt.), suggesting that the polar environment of the ionic crystal can have an effect on "soft" bonds similar to that of a polar solvent.[36] For all other geometrical parameters, theory and experiment also agree reasonably well, the only exception being the orientation of the Im group: As compared to the simulations in the gas phase or in solution, the dihedral angle θ adopts a much smaller value in the solid.

A more thorough investigation of the rotational profile of the Im group at the BP86/AE1 level showed the presence of a second minimum (**1′**, C_s-symmetry), in which the Im plane is eclipsed with the terminal VO bond ($\theta = 0°$). The transition state connecting both minima, **1TS**, is very close in energy to **1′** (less than 0.1 kcal/mol higher at BP86/AE1) and has a θ value of 25° (see Figure 1). Inclusion of diffuse functions and zero-point corrections actually reverses the energetic ordering between **1TS** and **1′**, and the rotational barrier passing through **1′** is only 0.4 kcal/mol (ΔE + ZPE level).[37]

When a CPMD simulation is started from **1′** in vacuo, the imidazole moiety immediately (that is, already in the 0.5 ps equilibration period) commences rotating, and continues to do so for the total simulation time. The saw-tooth steps in Figure 2a, an illustration of how θ evolves with time, are not indicating discontinuities, but are a consequence of the definition of this angle ranging from +180° to −180°. The rotational period of the imidazole unit is slightly longer than 1 ps.

From the very low barrier discussed above, essentially free rotation of the Im moiety is to be expected at ambient temperature. In the simulation starting from isolated **1**, apparently, no initial momentum is present that would induce an immediate rotation, and only relatively small variations in θ occur after equilibration (full lines in Figure 2a, after 0 ps). When the simulation is started from **1′**, the system is rapidly dragged toward the lower minimum, and the concomitant twist

(32) Troullier, N.; Martins, J. L. *Phys. Rev. B* **1991**, *43*, 1993−2006.
(33) Kleinman, L.; Bylander, D. M. *Phys. Rev. Lett.* **1982**, *48*, 1425−1428.
(34) Lee, C.; Yang, W.; Parr, R. G. *Phys. Rev. B* **1988**, *37*, 785−789.
(35) Reed, A. E.; Curtiss, L. A.; Weinhold, F. *Chem. Rev.* **1988**, *88*, 899−926.
(36) Cf. BH_3NH_3: Bühl, M.; Steinke, T.; Schleyer, P. v. R.; Boese, R. *Angew. Chem., Int. Ed. Engl.* **1991**, *30*, 1160−1161.
(37) There is another stationary point in C_s symmetry with $\theta = 180°$, which is a transition state 0.7 kcal/mol above **1**.

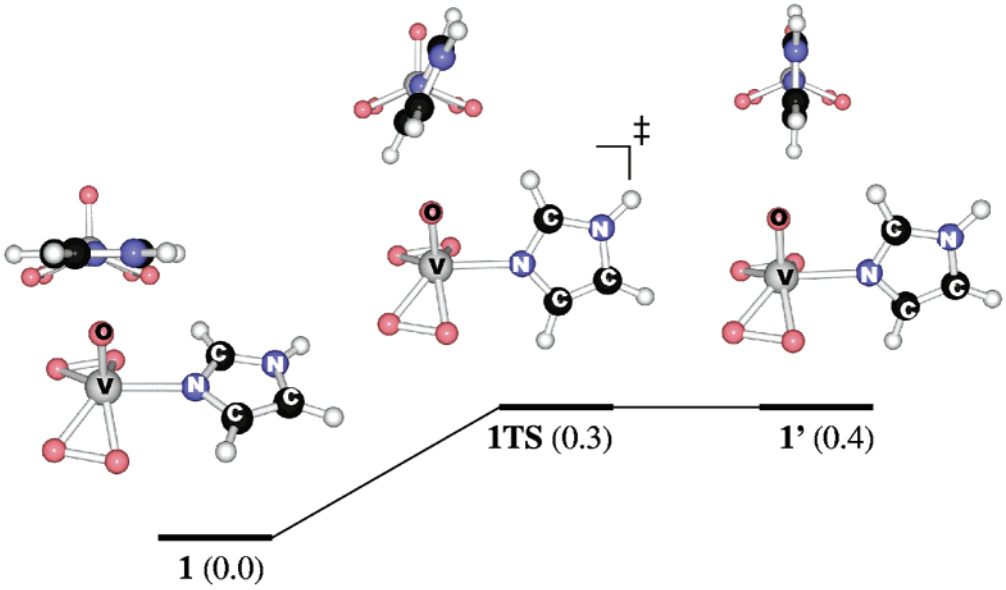

Figure 1. Stationary points involved in Im rotation in **1** (in parentheses: relative energies, ΔE + ZPE level); two views are shown in each case.

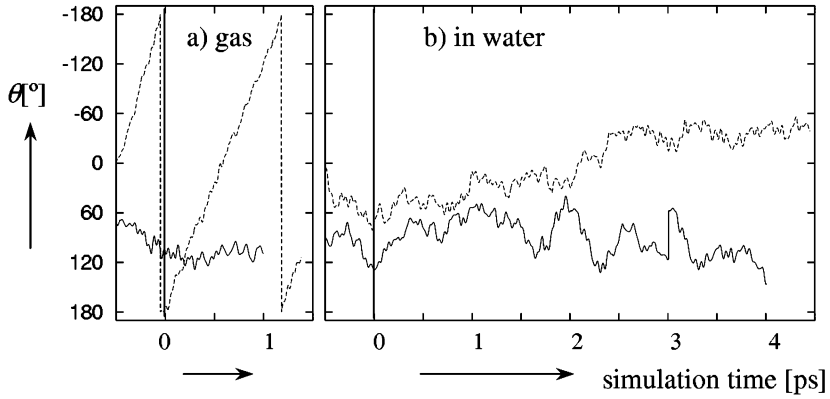

Figure 2. Variation of θ with time in CPMD simulations starting from **1** (full lines) and **1′** (dashed lines): left, in vacuo; right, in aqueous solution (including equilibration).

of the Im group provides such initial momentum that is sufficient to overcome the barrier anew after a full rotation. That the course of the simulation depends so strongly on the initial conditions (the starting structure in this case) indicates that true equilibration between the various internal vibrational degrees of freedom, in particular involving the very "soft" internal rotation, has not yet been reached. For the complex in the gas phase, the simulation starting from **1′** is probably the more realistic one, because this shows the free rotation expected from the low barrier.

Arguably, the dynamics in aqueous solution is more complicated. On one hand, collisions with solvent molecules could provide momenta that would induce Im rotation. In fact, much larger amplitudes are found for θ starting from **1** in water, as compared to the gas phase (full lines in Figure 2a and b). On the other hand, the solvent can serve to slow the rotation observed in the gas phase, due to water diffusing into the way of the rotating imidazole "wheel" or being held in place there by hydrogen bonds to the oxo or peroxo ligands at the metal. When a CPMD simulation was started from **1′** in water, indeed no free rotation is observed within several picoseconds. The amplitudes for θ are similar to those in the trajectory starting from **1** (compare dashed and full lines in Figure 2b). From the trend discernible in Figure 2b, a full Im rotation would be expected to require on the order of 10 ps or more.

Table 2. ^{51}V Chemical Shifts (B3LYP Level for BP86 Optimized or Simulated Geometries)[a] of **1** and $[VO(O_2)_2(OH_2)]^-$ (**2**)

level of approximation	**1**	**1′**	**2**	$(\Delta\delta)^b$
δ_e//BP86/AE1	−724	−650	−629	(95)
δ_e//CP-opt	−722	−649	−588	(134)
δ^{300K}//CPMD	−696	−685	−561	(135)
δ^{300K}//CPMD/D_2O	−833	−864	−682	(151)
experiment/H_2O[c]	−748		−692	(56)

[a] In ppm relative to $VOCl_3$; equilibrium (δ_e) and thermally averaged values (δ^{300K}), computed or averaged for the geometries obtained as indicated after the double slash. [b] Difference between **1** and **2**. [c] From ref 14 and: Rehder, D. In *Metal Ions in Biological Systems*; Sigel, H., Sigel, A., Eds.; M. Dekker, Inc.: New York, 1995; Vol. 31, p 1.

What are the effects of the molecular dynamics on the ^{51}V NMR chemical shifts? Equilibrium and dynamically averaged $\delta(^{51}V)$ values are summarized in Table 2. Fortuitously, the δ_e value for static **1** appears to fit best to experiment. Thermal averaging in the gas phase causes relatively small changes in the chemical shifts for **1** and **1′**, on the order of ca. 30 ppm (compare CP-opt and CPMD entries); a somewhat larger shielding effect (ca. 140−180 ppm) is obtained upon going from the gas phase into aqueous solution (compare CPMD and

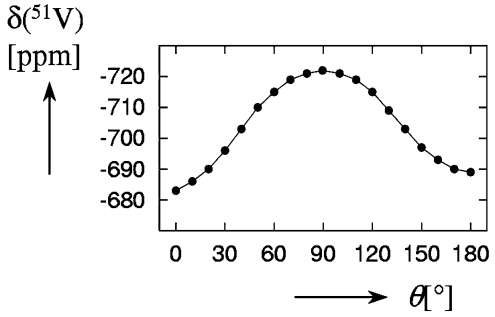

Figure 3. Variation of the computed ^{51}V chemical shift in **1** upon Im rotation.

CPMD/D_2O entries). The final ^{51}V chemical shift simulated in aqueous solution is too strongly shielded by ca. 100 ppm with respect to experiment. Errors of this magnitude are not uncommon for theoretical $\delta(^{51}V)$ values[38] and are relatively small as compared to the total chemical shift range of this transition metal, which covers several thousands of ppm.[18] Interestingly, almost all $\delta(^{51}V)$ values of vanadates and peroxovanadates simulated so far have been found systematically too low (too negative) as compared to experiment.[19a,20,39]

Results similar to those for **1** (notably a predicted shielding on going from the gas phase into water) have been obtained for the related peroxo complex $[VO(O_2)_2(OH_2)]^-$ (**2**, i.e., **1** with a water ligand instead of imidazole) based on CPMD/BLYP simulations.[19a] The analogous CPMD/BP86-derived data for **2** are included in Table 2.[40] The difference in $\delta(^{51}V)$ between **1** and **2** is reproduced by the simulations in a qualitatively correct manner (the metal is more shielded in **1** than in **2**), but quantitatively the trend is significantly overestimated (see $\Delta\delta$ values in parentheses in Table 2). The computed thermal and solvent effects on the metal shielding in **1** and **2** are very similar, so that effects on $\delta(^{51}V)$ of modifying the ancillary ligand can be assessed by static computations for the equilibrium geometries (see the Substituent Effects section below).

What factors govern the trends in $\delta(^{51}V)$ upon thermal averaging and solvation? The orientation of the Im group has been found to affect the EPR properties of vanadyl complexes noticeably.[41] To probe if ^{51}V chemical shifts could be of similar diagnostic value for the Im orientation in diamagnetic vanadium complexes, we have computed $\delta(^{51}V)$ in **1** as a function of the dihedral angle θ (Figure 3).[42] In fact, sizable variations of up to ca. 40 ppm are found, indicating that this single geometrical parameter is responsible for the major part of the difference between $\delta(^{51}V)$ in **1** and **1′** (ca. 70 ppm, see Table 2) with θ values of ca. 90° and 0°, respectively.

To gauge the importance of the VN bond length on the chemical shift, we have computed the corresponding bond-length shielding derivative in **1**,[42] arriving at a value of $\partial\sigma^V/\partial r_{VN} = -719$ ppm Å^{-1}. In absolute terms, this value is much smaller than those deduced or computed for other transition-metal complexes so far. For $[Co(CN)_6]^{3-}$, for example, an experimental estimate of $\partial\sigma^{Co}/\partial r_{CoC} = -8000$ ppm Å^{-1} (i.e., -1300 ppm Å^{-1} per bond) has been given on the basis of isotope effects on the metal chemical shift,[43] and for MnO_4^-, $\partial\sigma^{Mn}/\partial r_{MnO} = -17\,000$ ppm Å^{-1} (i.e., -4300 ppm Å^{-1} per bond) has been predicted.[19d] Even with the small r_{VN} shielding derivative in **1**, however, effects of this parameter are notable, because this bond length changes significantly upon solvation: The concomitant bond contraction in **1**, nearly 0.1 Å (see above), translates into a shielding of the metal of ca. 70 ppm, which is larger than possible effects due to Im rotation (Figure 3), and amounts to roughly one-half of the computed total gas-to-liquid shift of 137 ppm (compare CPMD and CPMD/D_2O entries in Table 2).

To summarize this section, the structure and properties of **1** have been investigated computationally using well-established DFT-based tools. Rotation of the Im group is facile, especially in the gas phase, and is somewhat slowed in solution. In general, the observed ^{51}V chemical shift and the geometrical parameters are well reproduced in the bulk simulations at ambient temperature.

(2) Olefin Epoxidation Catalyzed by 1. Oxygen transfer reactions of peroxides is an intensely researched area,[44] of which olefin epoxidation mediated by transition-metal complexes occupies a fair share. Computational studies of such epoxidation pathways abound,[45−50] but to our knowledge no investigations have been reported for vanadium species so far.[51]

From these studies, three possible pathways have emerged, which, adapted for **1**, are sketched in Scheme 2. Path 1 starts with coordination of H_2O_2 to the catalyst and formation of a hydroperoxy complex (**4**), which is the actual oxygen transfer agent. Such a mechanism, previously suggested by Sheldon,[52] has been favored for related $MoO(O_2)_2(L-L)$ complexes (where L−L denotes chelating bisnitrogen donors, as modeled by two ammonia ligands).[45d] Path 2 is initiated by direct oxygen transfer from the catalyst to the olefin, yielding a monoperoxo intermediate (**5**), which subsequently reacts with H_2O_2 to regenerate the catalyst. Such a pathway, originally put forward by

(38) Bühl, M.; Hamprecht, F. A. *J. Comput. Chem.* **1998**, *119*, 113−122.
(39) (a) Bühl, M. *J. Comput. Chem.* **1999**, *20*, 1254−1261. (b) Bühl, M. *J. Inorg. Biochem.* **2000**, *80*, 137−139.
(40) The simulations with the BLYP or the BP86 functionals afford very similar qualitative results, for example, for the averaged V−O(H_2) bond length: On going from the gas phase into aqueous solution, this bond contracts from 2.279 to 2.017 Å, that is, by 0.26 Å, at the BP86 level (present work), and from 2.394 to 2.082 Å, that is, by 0.31 Å, with the BLYP functional (ref 19a).
(41) (a) Smith, T. S., II; Root, C. A.; Kampf, J. W.; Rasmussen, P. G.; Pecorano, V. L. *J. Am. Chem. Soc.* **2000**, *122*, 767−775. (b) Saladino, A. C.; Larsen, S. C. *J. Phys. Chem. A* **2002**, *106*, 10444−10451.
(42) From a rigid scan with all other parameters fixed to the values in the CP-opt geometry of **1**.
(43) Jameson, C. J.; Rehder, D.; Hoch, M. *J. Am. Chem. Soc.* **1987**, *109*, 2589−2594. This empirical value has been qualitatively reproduced using theoretical methods similar to those employed in the present study, see: Godbout, N.; Oldfield, E. *J. Am. Chem. Soc.* **1997**, *119*, 8065−8069.
(44) Adam, W., Ed. *Peroxide Chemistry*; Wiley-VCH: Weinheim, 2000.
(45) Mo, for example: (a) Kühn, F. E.; Groarke, M.; Bencze, E.; Prazeres, A.; Santos, A. M.; Calhorda, M. J.; Romao, C. C.; Goncalves, I. S.; Lopes, A. D.; Pillinger, M. *Chem.-Eur. J.* **2002**, *8*, 2370−2383. (b) Deubel, D. V.; Sundermeyer, J.; Frenking, G. *Eur. J. Inorg. Chem.* **2001**, 1819−1827. (c) Deubel, D. V.; Sundermeyer, J.; Frenking, G. *Org. Lett.* **2001**, *3*, 329−332. (d) Hroch, A.; Gemmecker, G.; Thiel, W. R. *Eur. J. Inorg. Chem.* **2000**, 1107−1114. (e) Deubel, D. V.; Sundermeyer, J.; Frenking, G. *J. Am. Chem. Soc.* **2000**, *122*, 10101−10108.
(46) Re: (a) Gisdakis, P.; Yudanov, I. V.; Rösch, N. *Inorg. Chem.* **2001**, *40*, 3755−3765. (b) Görling, A.; Trickey, S. B.; Gisdakis, P.; Rösch, N. *Top. Organomet. Chem.* **1999**, *4*, 109−164.
(47) Mn: (a) Cavallo, L.; Jacobsen, H. *J. Org. Chem.* **2003**, *68*, 6202−6207. (b) Adam, W.; Roschmann, K. J.; Saha-Möller, C. R.; Seebach, D. *J. Am. Chem. Soc.* **2002**, *124*, 5068−5073.
(48) Cr: Rappe, A. K.; Li, S. *J. Am. Chem. Soc.* **2003**, *125*, 11188−11189.
(49) Ti: (a) Sever, R. R.; Root, T. W. *J. Phys. Chem. B* **2003**, *107*, 4090−4099. (b) Cui, M.; Adam, W.; Shen, J. H.; Luo, X. M.; Tan, X. J.; Chen, K. X.; Ji, R. Y.; Jiang, H. L. *J. Org. Chem.* **2002**, *67*, 1427−1435.
(50) Fe: (a) Musaev, D. G.; Basch, H.; Morokuma, K. *J. Am. Chem. Soc.* **2002**, *124*, 4235−4148. (b) de Visser, S. P.; Ogliaro, F.; Harris, N.; Shaik, S. *J. Am. Chem. Soc.* **2001**, *123*, 3037−3047.
(51) For a recent study of the oxidation of ethylene by coordinatively unsaturated VO_2^+, see: Garcia, L.; Sambrano, J. R.; Safont, V. S.; Calatayud, M.; Beltrán, A.; Andrés, J. *J. Phys. Chem. A* **2003**, *107*, 3107−3120.
(52) Sheldon, R. A. *Recl. Trav. Chim. Pays-Bas* **1973**, *253*, 367.

Scheme 2. Possible Catalytic Cycles for Ethylene Epoxidation with **1**

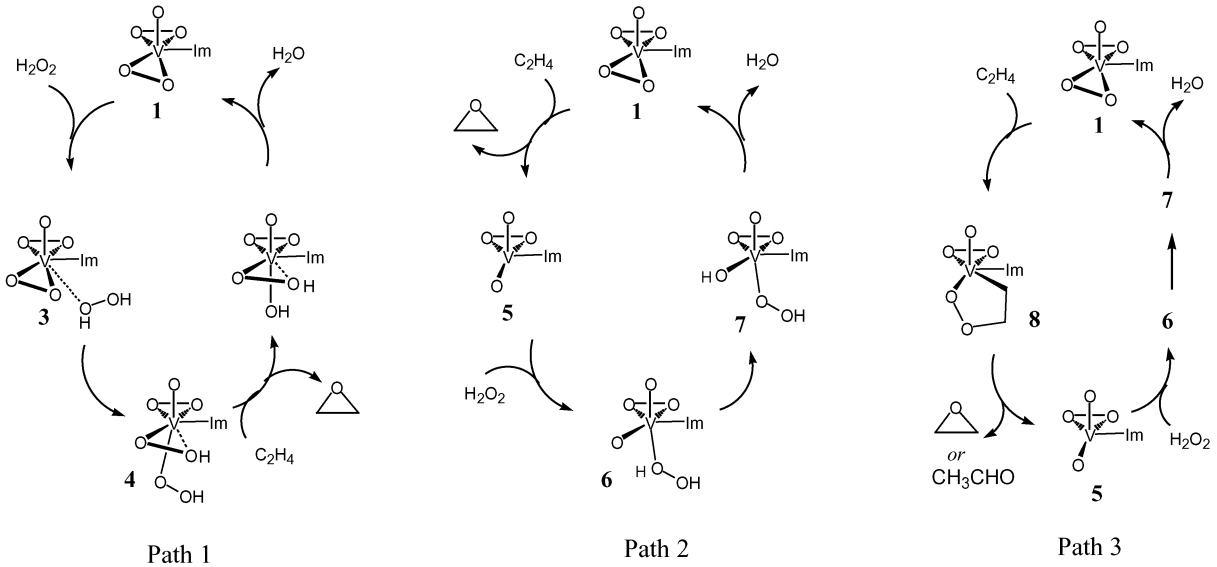

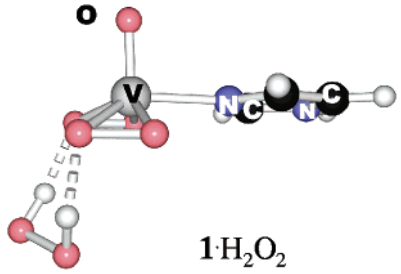

Figure 4. BP86/AE1 optimized structure of **1**·H_2O_2 (side view).

Sharpless,[53] has been confirmed computationally for several Mo and Re analogues, for example, $ReO(O_2)_2(CH_3)(OH_2)$.[46a] Entry in Path 3 is accomplished by insertion of the olefin into a metal−oxygen bond under formation of a transient metalla-2,3-dioxolane (**8**), which decomposes − under liberation of the reaction products − to the same monoperoxo intermediate **5** from Path 2. Such a mechanism has been suggested to be operative with $MoO(O_2)_2(hmpa)$[54] and has been computed for a smaller model with OPH_3 as coligand.[45e] In the following, all three pathways are scrutinized starting from **1**.

The initial step in Path 1 is coordination of H_2O_2 to the vanadium center in **1**. All attempts to locate a corresponding minimum (**3** in Scheme 2) failed, however. The additional ligand was always expelled from the coordination sphere of the metal and remained hydrogen-bonded to the two peroxo moieties. The lowest minimum is displayed in Figure 4. The same happened when a CPMD run was started by placing **3** in a periodic water box.

Likewise, no minimum corresponding to **4** could be found. All optimizations starting from an arrangement as depicted in Scheme 2 resulted in dissociation of the imidazole ligand from the complex.[55] Apparently, the metal center in **1** is very reluctant to increase its coordination number beyond six. A number of seven-coordinated $VO(O_2)_2$ complexes have been characterized by X-ray crystallography, but without exception these contain chelating ligands with strong donors (aromatic N atoms and/or carboxylato groups).[56] A monodentate ligand such as Im produces six-coordinate species.[14] In contrast, essentially all neutral complexes with the $MoO(O_2)_2$ fragment have a coordination number of seven about Mo, irrespective of the denticity of the ligands.[57] It is particularly noteworthy that the Mo analogue of **1**, $MoO(O_2)_2(Im)(OH_2)$, is seven-coordinated with an additional water molecule trans to the oxo ligand.[58] H_2O molecules are also present in the solid containing **1**, but only as crystal water, not coordinated to vanadium.[14] A possible reason for this difference in stereochemistry is the smaller size of vanadium as compared to molybdenum, which increases mutual repulsion of the ligands. In addition, the vanadium complex is anionic,[59] with a large fraction of the negative charge at the terminal oxo ligand (−0.6*e* according to natural population analysis at the BP86/AE1+ level), thereby increasing the trans-influence of the latter. As a consequence, the availability of the seventh coordination site is considerably reduced. Thus, Path 1 can be viable for neutral peroxo-molybdenum complexes,[45d] but not for the corresponding anionic vanadium congeners.

Turning now to Path 2, we have located the transition state for oxygen transfer from **1** to the substrate, affording the epoxide and monoperoxo complex **5**. This step proceeds via a spiro-like transition transition structure, **TS15** (see Figure 5), and requires only a moderate activation energy, 17.3 kcal/mol (ΔE + ZPE level, 27.8 kcal/mol at ΔG^{298}). Similar structures and barriers have also been reported for the related Mo species.[45e,46a] The O atom is approaching the olefin in a rather unsymmetrical fashion, with the two forming C−O bonds differing by 0.57 Å

(53) Sharpless, K. B.; Townsend, J. M.; Williams, D. R. *J. Am. Chem. Soc.* **1972**, *94*, 295.
(54) Mimoun, H.; Seree de Roch, I.; Sajus, L. *Tetrahedron* **1970**, *26*, 37.
(55) In the gas phase, the imidazole is also not strongly bound in **1**, as the dissociation energy (for the reaction **1** → $[VO(O_2)_2]^-$ + Im) is computed to be only 10.7 kcal/mol at the BP86/AE1 level. It has been noted in part 1, however, that in aqueous solution the bonding between V and Im is substantially reinforced (see V−N bond lengths in Table 1).
(56) For example, $[VO(O_2)_2(bipy)]^-$, where the N atom trans to the oxo ligand is more weakly bound (r_{VN} = 2.29 Å) than the equatorial N atom (r_{VN} = 2.15 Å): Szentivanyi, H.; Stomberg, R. *Acta Chem. Scand. A* **1983**, *37*, 553.
(57) For example, $MoO(O_2)_2(OH_2)_2$: Shoemaker, C. B.; Shoemaker, D. P.; McAfee, L. V.; DeKock, C. W. *Acta Crystallogr., Sect. C* **1985**, *41*, 347.
(58) Martin-Zarza, P.; Gili, P.; Rodriguez-Romero, P. V.; Ruiz-Peres, C.; Solans, X. *Inorg. Chim. Acta* **1994**, *223*, 173.
(59) Interestingly, the only mononuclear, six-coordinated Mo analogue structurally characterized so far is also an anion, $[MoO(O_2)_2(OSiPh_3)]^-$: Piquemal, J.-Y.; Halut, S.; Brégeault, J.-M. *Angew. Chem., Int. Ed.* **1998**, *37*, 1146−1149.

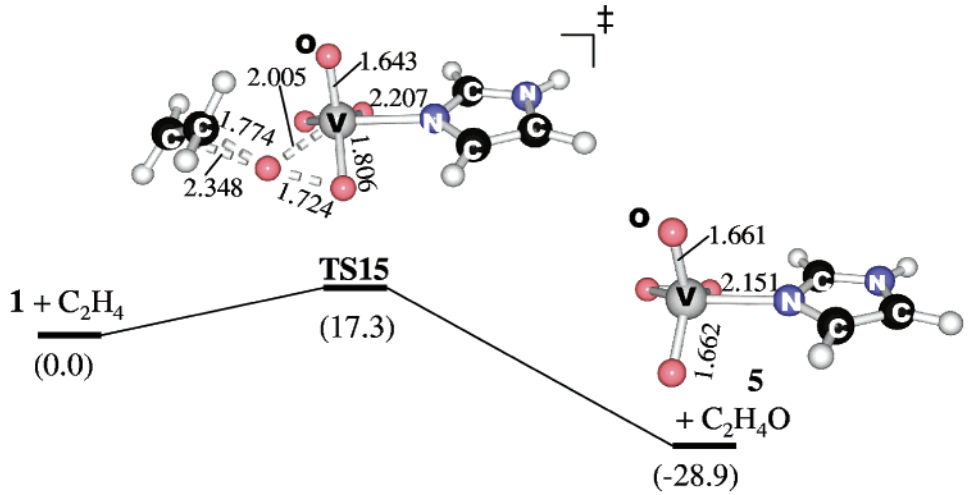

Figure 5. Entry into Parth 2 via oxygen transfer, including key distances (in Å), optimized at the BP86/AE1 level, and relative energies (in kcal/mol, ΔE + ZPE level).

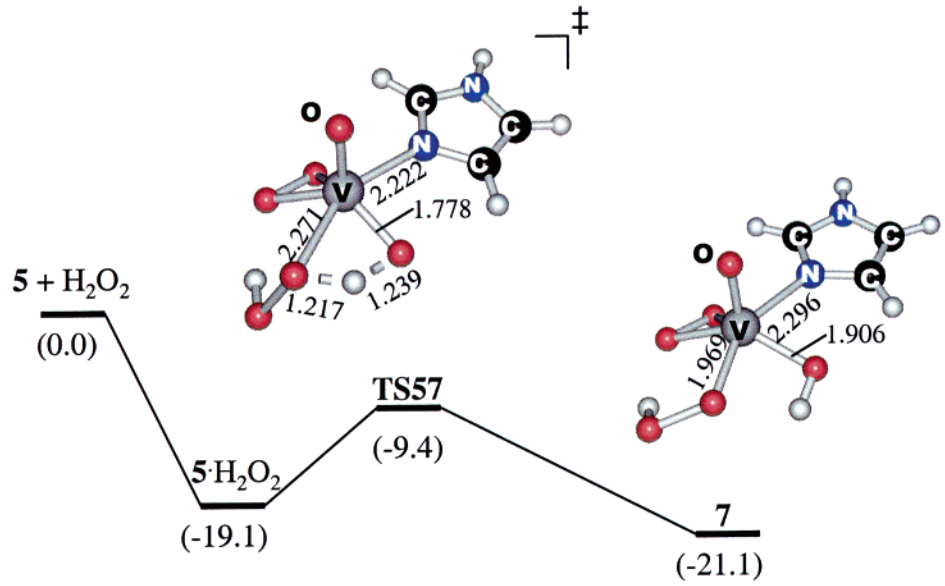

Figure 6. Initial step for regeneration of catalyst **1** by H_2O_2 addition to **5**; key distances (in Å), optimized at the BP86/AE1 level, and relative energies are included (in kcal/mol, ΔE + ZPE level, counterpoise-corrected for **5**·H_2O_2).

in **TS15** (Figure 5). A tendency toward asynchronous oxygen transfer had also been noted in related Mo systems, where the two forming C−O bonds differ by up to 0.11 Å, for example, in $Mo(O_2)_2(OPH_3)$.[45e] Such asymmetry might be expected for a radical-type mechanism, for example, involving a transient $V^{IV}-O-O-CH_2-CH_2\cdot$ species, but no evidence was found for such an electronic structure in **TS15**: the restricted wave function turned out to be stable, and no lower open-shell solutions could be found. Oxygen transfer thus proceeds asynchronous, but concerted.

In the numbering scheme of Scheme 1, it is O3 that is transferred to the olefin in **TS15**. The remaining three transition states for transfer of any of O2, O4, or O5 have also been located, but have been found to be higher in energy by 2.9−6.4 kcal/mol at the BP86/AE1 level.[60]

The driving force for this first step, that is, **1** + C_2H_4 → **5** + C_2H_4O, is considerable, ca. −29 kcal/mol in the gas phase (−27.9 kcal/mol at ΔG^{298}). The reaction product, monoperoxo species **5**, is stable over several picoseconds in a CPMD simulation in water, where no spontaneous decay occurs, for example, by way of reaction with the solvent. Reaction of **5** with H_2O_2 is not initiated by coordination of the latter to the metal. All attempts to optimize such a complex in the gas phase resulted in expulsion of the hydrogen peroxide from the coordination sphere, affording a simple H-bonded adduct (as was the case for **1** + H_2O_2, see above). We also performed extensive CPMD simulations in water, but in no case did H_2O_2 remain in the coordination sphere of **5**.

It turned out that at the BP86 level in the gas phase, H_2O_2 can add metathetically to **5** under cleavage of one of its OH bonds.[61] The transition state that has been located (**TS57**, Figure 6) is actually lower in energy than the separated reactants. This is because the transition state does not connect to the separated reactants, but to the doubly H-bonded complex of both (**5**·H_2O_2,

(60) The barrier for transfer of the oxo ligand O1 to the olefin is much higher, ca. 60 kcal/mol (BP86/AE1 + ZPE level).

(61) The product of this process, hydroperoxy complex **7**, is a stable minimum, unlike the elusive hydroperoxy complex **4**, which would have a higher coordination number (see Scheme 2).

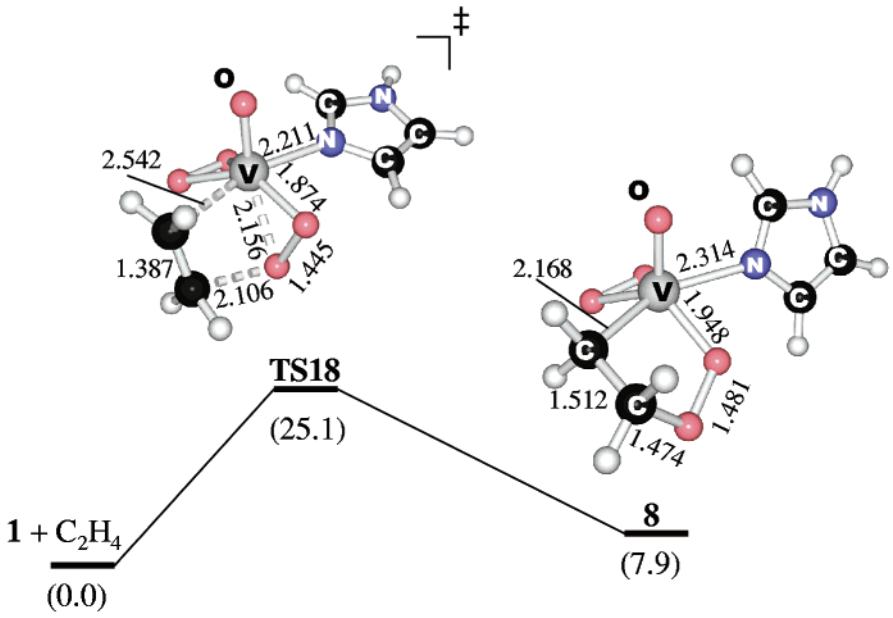

Figure 7. Entry into Path 3 via olefin insertion, including key distances (in Å), optimized at the BP86/AE1 level, and relative energies (in kcal/mol, ΔE + ZPE level).

not shown in Figure 6), which is a strongly stabilized ion−dipole complex; **TS57** lies 9.7 kcal/mol above this complex (ΔE + ZPE). In aqueous solution, there also appears to be a barrier for this process, as no spontaneous OH activation was observed in the simulations. We have not attempted to assess the height of this barrier with CPMD simulations (e.g., via thermodynamic integration over several constrained MD runs), as a much smaller activation energy than that of olefin epoxidation via **TS15** and, thus, a very facile reaction is to be expected. This expectation is corroborated by an estimate of bulk solvent effects using a polarizable continuum model,[62] together with a molecule-shaped cavity and the parameters of water. When single-point energy calculations are performed with such an approach, the oxo-transfer barrier (i.e., **TS15** relative to **1**) is 17.7 kcal/mol (BP86/AE1+ level), that is, very similar to the gas-phase value (17.3 kcal/mol, Figure 5), and **TS57** is 5.5 kcal/mol above **5** + H_2O_2. Thus, the latter step should proceed much more facile than the former.

In water, there are probably many possible pathways for H_2O elimination leading from **7** back to **1**, some of which are most probably solvent-assisted, and it is unlikely that this reaction would be a bottleneck in the catalytic cycle. In the gas phase, we were able to locate a transition state for water elimination from **7**, but surprisingly this did not lead to **1**, but rather to a somewhat exotic, cyclic intermediate (**9**, Scheme 3), which then can rearrange to **1**.[63] On the zero-point corrected potential energy surface, the total activation barrier for this pathway (i.e., between **7** and **TS91**) is somewhat higher than that of the epoxidation step via **TS15**. When entropy effects are taken into account, however (see below), the latter barrier is higher and is thus the rate-determining one. These results do not imply that **9** would

Scheme 3. Possible Pathway for Transformation of **7** Back to **1** (in Parentheses: Relative Energies at the ΔE + ZPE Level)

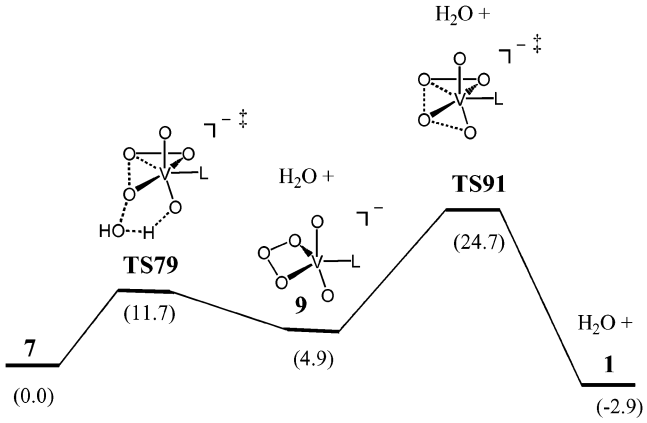

actually be part of a catalytic cycle in solution. We report these data for completeness and without further discussion, just to show that even in the absence of solvent, the epoxidation step would be rate-limiting.[64]

Finally, we have explored computationally if initial olefin insertion (Path 3 in Scheme 2) could be competitive with initial oxo transfer, as has been discussed for related Mo species.[45e] After product elimination from the initially formed metalla-dioxolane **8**, this path would connect to the second part of Path 2 with **5** as common intermediate. We have located a transition state for ethylene insertion into a peroxide−VO bond (**TS18** in Figure 7), affording **8**. The resulting barrier, 25.1 kcal/mol (ΔE + ZPE level, 36.9 kcal/mol at ΔG^{298}), is much higher than that for oxo transfer via **TS15** (Figure 5). In addition, the insertion product **8** is higher in energy than the separated reactants. Thus, entry into Path 3 is both kinetically and thermodynamically

(62) As implemented in Gaussian 98, cf.: (a) Miertus, S.; Scrocco, E.; Tomasi, J. *Chem. Phys.* **1981**, *55*, 117−129. (b) Mennucci, B.; Tomasi, J. *J. Chem. Phys.* **1997**, *106*, 5151−5158. (c) Barone, V.; Cossi, M.; Tomasi, J. *J. Chem. Phys.* **1997**, *107*, 3210−3221. Review: (d) Tomasi, J.; Persico, M. *Chem. Rev.* **1994**, *94*, 2027−2094.

(63) We explored a few other possibilities, such as proton transfer from the hydroperoxo to the hydroxo group in **7**, but no transition state lower in energy than **TS79** was found.

(64) A referee pointed out that **9** could decompose through other channels, for example, elimination of singlet dioxygen. This process, that is, **9** → $[VO_2Im]^-$ + $^1O_2$, is computed to be quite endothermic in the gas phase, ΔE = +19.7 kcal/mol at the BP86/AE1 level (obtained from the calculated reaction energy using $^3O_2$ and adding the experimental energy difference between $^3O_2$ and $^1O_2$, 22 kcal/mol). Elimination of ozone is indicated to be even less favorable.

Scheme 4. Evolution of Free Energy ΔG^{298} (in Parentheses, kcal/mol Relative to **1**) along Path 2 and Entry into Path 3

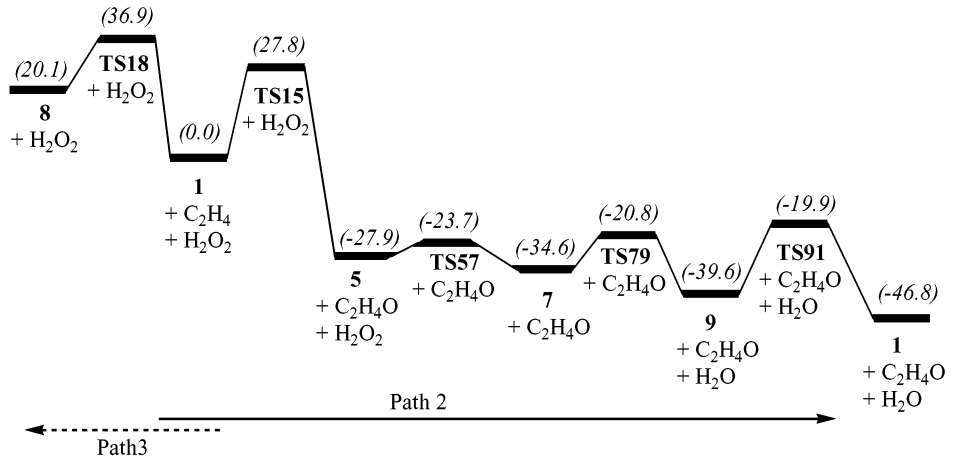

disfavored over that into Path 2 and can be excluded for peroxovanadate **1**.[65]

Thus far, mainly relative energies on the potential energy surface have been discussed. The free energy profiles at room temperature (ΔG^{298}) of the first part of Path 3 and that of the entire Path 2 are summarized in Scheme 4. It should be kept in mind that the enthalpic and, in particular, the entropic contributions evaluated from the ideal-gas assumption are only a rough guide and may be somewhat attenuated in solution. The qualitative conclusions should be reliable, however, in particular, the preference of Path 2 over Path 3. The latter is even more disfavored at the ΔG level than at ΔE + ZPE (cf., Figure 7). On Path 2, the initial oxo transfer is rate-limiting because it not only passes over the highest point in total, but has also the highest barrier of each elementary step (i.e., with respect to the preceding minimum). Once the first barrier is overcome, the remaining sequence should thus proceed smoothly, in particular because there is a consecutive lowering of the free energy on going from each intermediate to the next one. Oxo transfer has also been computed to be rate-limiting in the oxidation of sulfides catalyzed by peroxovanadium species.[66]

(3) Substituent Effects. The next question after identification of the reaction path and the rate-determining step is, how is the activation barrier of this step affected by the nature of the ligands attached to the metal? Imidazoles, and nitrogen-containing heterocycles in general, are versatile ligands in transition-metal chemistry, and a plethora of derivatives of the various motifs is known.[67] To study electronic effects of substituents on the oxo-transfer barrier, we have replaced the Im moiety in **1** and **TS15** by the ligands shown in Table 3. These comprise imidazole derivatives with a donor or an acceptor group attached (Cl and NO_2, respectively), or deprotonated at Im, other aromatic N-donor ligands such as pyrazole and pyridine, as well as two examples with formally sp^3- and sp-hybridized N atoms (ammonia and acrylnitrile, respectively).

Most ligands afford very similar barriers around ca. 16 kcal/mol, indicative of little overall sensitivity of this property toward subtle electronic effects. There are notable exceptions, however: The strongly electron-withdrawing nitro-substituent in **11** leads to a significant increase in the barrier, by almost 3 kcal/mol. This comes as a surprise because an electron-withdrawing group should facilitate electrophilic attack at the olefin, as has for instance been observed in epoxidations using Mo-based catalysts with chelating ligands.[68] Unfortunately, no simple explanation for this counterintuitive result can be put forward.

A substantial decrease in the barrier, by 6 kcal/mol with respect to the parent system **1**, is found upon deprotonation of the Im moiety (**12** in Table 3). This finding will be dicussed in more detail below. A somewhat less pronounced decrease, by 2 kcal/mol, is found upon substituting Im for the pyrazole ligand (**13**).

In context with these substituent effects, we were interested to see if this system could be another example of an NMR/

Table 3. Effect of Variation of L in $[VO(O_2)_2L]^-$ on the Oxo-Transfer Barrier ΔE and the ^{51}V Chemical Shift

-L		ΔE^a	$\delta(^{51}V)^b$
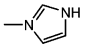	(**1**)	16.6	-724 *(-748)*[c]
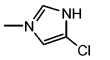	(**10**)	16.6	-724
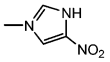	(**11**)	19.4	-761
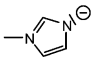	(**12**)	10.6	-758
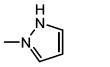	(**13**)	14.6	-700
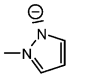	(**14**)	9.1	-733
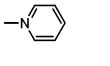	(**15**)	16.5	-710 *(-712)*[d]
–N≡C-Me	(**16**)	16.6	-670
$-NH_3$	(**17**)	16.2	-705

[a] In kcal/mol, BP86/AE1+//BP86/AE1 level. [b] Gas-phase equilibrium value, GIAO-B3LYP/AE1+//BP86/AE1 level (experimental solution value in parentheses). [c] From ref 14. [d] Tracey, A. S.; Jaswal, J. S. *Inorg. Chem.* **1993**, *32*, 4235−4243.

(65) For Mo species following the insertion pathway, an additional reaction channel would be accessible, elimination of acetaldehyde rather than the epoxide from the metalla-oxalane (cf., ref 45e); we did not explore this possibility for **8**, as its formation is strongly disfavored in the first place.
(66) Balcells, D.; Maseras, F.; Lledós, A. *J. Org. Chem.* **2003**, *68*, 4265−4274.
(67) For instance Im derivatives: Sundberg, R. J.; Martin, R. B. *Chem. Rev.* **1974**, *74*, 471−517.
(68) Thiel, W. R.; Eppinger, *J. Chem.-Eur. J.* **1997**, *5*, 696−705.

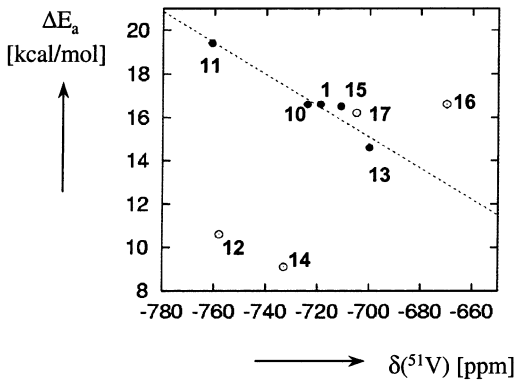

Figure 8. Correlation of the computed $\delta(^{51}V)$ and ΔE^a values from Table 3. A linear fit for the neutral aromatic heterocycles (solid circles) is shown.

reactivity correlation. For a number of catalytic[69] and stoichiometric[70] reactions at transition-metal centers, it has been possible to correlate reactivities or catalytic activities with the chemical shifts of the metal.[71] When such a correlation is established within a series of closely related compounds, it could be possible, for instance, to select prospective catalysts on the basis of their NMR spectra. A few such correlations have been rationalized or predicted computationally.[72]

From the plot of the computed activation barriers versus ^{51}V chemical shifts in Figure 8, an overall trend toward a lower barrier with a more deshielded metal can be discerned for the neutral heterocyclic ligands (solid circles). This correlation, however, does not extend to the formally sp-hybridized donor (**16**) or the deprotonated Im and pyrazole ligands (**12** and **14**, respectively). Thus, no general NMR/reactivity correlation can be predicted, and a screening of prospective catalysts by ^{51}V NMR spectroscopy would not appear to be reliable.

The remarkably low barrier in the deprotonated species **12**, however, may serve as a lead for further rational ligand design. The imidazolate anion is a stronger base and a better donor than neutral imidazole. The concomitant stabilization of the peroxovanadate fragment is not so much apparent in the ground-state structures (e.g., on going from **1** to **12** the VN bond decreases just by 0.004 Å), but comes to the fore in the transition states: upon removal of the proton at Im in **TS15**, the bonding to the N-donor is considerably reinforced, as evidenced by a substantial VN bond contraction (by 0.05 Å) and a notable increase in the Wiberg bond index,[73] a measure of the covalent bond order, from 0.29 to 0.39 (from natural population analysis at the BP86/AE1+ level). At the same time, the asymmetry of the ethylene moiety with respect to the incoming O atom increases upon deprotonation (cf., the CO distance pairs change from 1.77/2.35 to 1.63/2.44 Å), as does the buildup of negative charge at the distant C atom of the olefin (from $-0.53e$ to $-0.75e$). It is probably this partial delocalization of the additional negative charge from the ligand onto the olefin which is responsible for the lowering of the barrier on going from **1** to **12**.

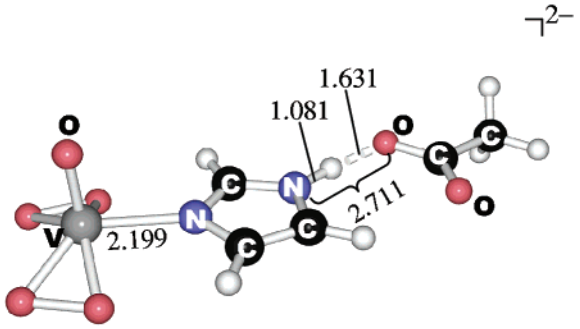

Figure 9. BP86/AE1 optimized structure of **1**·OAc$^-$ including key distances (in Å).

Full deprotonation of free Im is not possible in water (cf., the estimated pK_a value of 14.2).[74] However, coordination of Im to a transition-metal fragment can lower the acid constant by several pK_a units,[75] cf., 10.9 in $[Fe(CN)_5Im]^{2-}$.[75a] Very basic conditions, however, would probably still be required to produce free **12** in aqueous solution. To probe to what extent the electronic structure of free **12** can be approached under less dramatic, that is, more biomimetic conditions, we have optimized a complex of **1** with a H-bond acceptor attached to the Im moiety, acetate ion in this case. The resulting **1**·OAc$^-$ (Figure 9) has the structural characteristics of a strong hydrogen bond, a significantly elongated NH distance (1.08 Å) and a short N···O separation (2.71 Å). Indeed, the oxo-transfer barrier of **1**·OAc$^-$ is appreciably reduced relative to that of **1**, by 2.7 kcal/mol (BP86/AE1+ level), albeit not as much as in the fully deprotonated system **12**. However, this result suggests that the activity of (imidazole)peroxovanadium complexes in bioinspired oxidation reactions could be significantly enhanced by attaching a suitable hydrogen-bond acceptor to the imidazole ligand.

It is tempting to speculate if a similar mechanism could be operative in the active center of the vanadium-dependent haloperoxidases. In the peroxo form that has been structurally characterized,[12b] the His residue coordinated to the vanadium center (HIS496) is indicated to form a hydrogen bond to the carboxylate group of a nearby asparagic acid (ASP500). The observed short and, thus, probably H-bonded N···O distance, 2.82 Å, is of the same order of magnitude as that optimized for **1**·OAc$^-$ (2.71 Å, Figure 9). Based on the results just discussed, this hydrogen bond could be critical for the activity of the enzyme. The importance of the hydrogen-bond network around the prosthetic group has been highlighted recently.[76] We have now provided computational evidence for the mode of action of one H-bond of this array, suggesting that, in the design of new biomimetic catalysts, this structural feature should be included.

Finally, we note that, as for Im, deprotonation of the pyrazole ligand in **13** results in a substantial decrease of the barrier, to ca. 9 kcal/mol (compare entries **13** and **14** in Table 3). We did

(69) (a) Bönnemann, H.; Brijoux, W.; Brinkmann, R.; Meurers, W.; Mynott, R.; von Philipsborn, W.; Egolf, T. *J. Organomet. Chem.* **1984**, *272*, 231. (b) Fornika, R.; Görls, H.; Seeman, B.; Leitner, W. *J. Chem. Soc., Chem. Commun*. **1995**, 1479−1480.
(70) For example: (a) DeShong, P.; Slough, G. A.; Sidler, D. R.; Rybczynski, P. J.; von Philipsborn, W.; Kunz, R. W.; Bursten, B. E.; Clayton, T. W. J. *Organometallics* **1989**, *8*, 1381−1388. (b) Koller, M.; von Philipsborn, W. J. *Organometallics* **1992**, *11*, 467−468.
(71) Review: von Philipsborn, W. *Chem. Soc. Rev.* **1999**, 95−106.
(72) (a) Bühl, M. *Organometallics* **1997**, *16*, 261−267. (b) Bühl, M. *Angew. Chem., Int. Ed.* **1998**, *37*, 142−144. (c) Bühl, M. *Organometallics* **1999**, *18*, 4894−4896.
(73) Wiberg, K. *Tetrahedron* **1968**, *24*, 1083−1096.
(74) George, P.; Hanania, G. I. H.; Irvine, D. H.; Aber-Issu, *J. Chem. Soc.* **1964**, 5689−5694.
(75) (a) Johnson, C. R.; Shepherd, R. E.; Marr, B.; O'Donnell, S.; Dressick, W. *J. Am. Chem. Soc.* **1980**, *102*, 6227−6235. (b) Hoq, M. F.; Shepherd, R. E. *Inorg. Chem*. **1984**, *23*, 1851−1858. (c) Review: Sjoberg, S. *Pure Appl. Chem*. **1997**, *69*, 1549−1570.
(76) Plass, W. *Coord. Chem. Rev*. **2003**, *237*, 205−212.

not probe the effect of attaching a H-bond acceptor to the corresponding proton in **13**, as this appears to be less favorable than in **1**·OAc^-, based on steric grounds.

Conclusion

We have presented a computational study of $[VO(O_2)_2(Im)]^-$ (**1**), which may serve as a model for vanadium-dependent haloperoxidases and their oxidative chemistry. Special attention is called to theoretical modeling of the ^{51}V chemical shift in aqueous solution and to the computational characterization of the pathway for olefin epoxidation. For the former property, the CPMD-based approach introduced previously has been applied. The quantitative accord with experiment of the dynamically averaged $\delta(^{51}V)$ values is not improved over that of the equilibrium values from simple, static calculations. However, interesting insights into internal dynamics of **1** and the consequences on the NMR parameter are obtained. Rotation of the coordinated imidazole moiety about the VN axis is indicated to be very rapid in the gas phase and is somewhat slowed in aqueous solution. This rotation affects the ^{51}V chemical shift noticeably, but even more important for this property is the VN bond length, which is considerably shortened upon going from the gas phase into aqueous solution.

For the mechanism of catalyic ethylene epoxidation, the path initiated by oxo transfer from **1** to the olefin is clearly favored over other mechanistic alternatives that have been considered. A complete catalytic cycle has been characterized, and the initial oxo transfer step via an asymmetric, spiro-like transition state is indicated to be rate-limiting, with a barrier of 17.3 kcal/mol (ΔE + ZPE level, 27.8 kcal/mol at ΔG^{298}).

Substituent effects on this barrier have been explored computationally by substituting the imidazole ligand in **1** with derivatives thereof, or with other N-donors. While an overall trend toward lower barriers with a more deshielded metal has been noted for the subset of neutral *N*-heterocycles, no general NMR/reactivity correlation is apparent. Of particular interest is the finding that the rate-limiting barrier is substantially reduced (by 6 kcal/mol) upon deprotonation of the imidazole ligand. A similar effect, albeit somewhat attenuated, is predicted when this proton is involved in a hydrogen bond to an acceptor such as acetate. There is evidence for such a H-bond in the solid-state structure of a vanadium-containing haloperoxidase, where it may be critical for the oxidative activity. This possibility has important implications for the design of new biomimetic catalysts with the peroxovanadate motif.

Acknowledgment. M.B. wishes to thank Prof. Walter Thiel and the Deutsche Forschungsgemeinschaft for continuing support, and Prof. Werner R. Thiel for helpful comments. A Humboldt fellowship for R.S. is gratefully acknowledged. Computations were performed on Compaq XP1000 and ES40 workstations at the MPI Mülheim, and on a Hitachi-SR8000 at the Leibniz Rechenzentrum in Munich, where a generous allotment of CPU time was granted.

Supporting Information Available: BP86/AE1 optimized Cartesian coordinates (ASCII text). This material is available free of charge via the Internet at http://pubs.acs.org.

JA039436F